ADVANCED MATERIALS
www.advmat.de

Achieving the 1D Atomic Chain Limit in Van der Waals Crystals

*Jordan Teeter, Na Yeon Kim, Topojit Debnath, Nicholas Sesing, Tekwam Geremew, Dylan Wright, Miaofang Chi, Adam Z. Stieg, Jianwei Miao, Roger K. Lake, Tina Salguero, and Alexander A. Balandin**

Experiments with graphene have demonstrated that 2D van der Waals materials can be stable, robust, and efficiently manipulated at the level of individual atomic planes. However, the stability and manipulation of 1D van der Waals materials and individual atomic chains remains elusive. Here, the ability to exfoliate and process two representative van der Waals materials containing 1D motifs, namely MoI_3 and Ta_2Se_8I, at the scale of individual atomic chains is demonstrated. High-resolution transmission electron microscopy and atomic force microscopy studies confirm the presence of stable individual atomic chains of MoI_3 at room temperature. It is further shown that 1D van der Waals materials with low exfoliation energy, such as Ta_2Se_8I, can be processed with electron beams to achieve suspended individual atomic chains. Ab initio calculations corroborate the findings regarding the cleavage energies and the thermodynamic stability of individual atomic chains in these 1D van der Waals materials. These results demonstrate that the top-down approach in material processing can be extended to the scale of individual chains.

1. Introduction

The thermodynamic stability of strictly 2D and 1D crystals is the subject of a long-standing debate originated from the works of Peierls[1] and Landau.[2] It follows from the harmonic approximation that the thermal fluctuations destroy the long-range order, leading to the melting of a 2D lattice at any finite temperature. According to the Mermin–Wagner theorem, the long-wavelength fluctuations destroy the long-range order of 2D crystals.[3] In other words, the thermal population of long-wavelength out-of-plane, i.e. flexural acoustic phonons, in 2D systems diverges at any finite temperature. This reasoning was subsequently extended to 1D crystals in the context of magnetic materials.[4] The exfoliation of graphene reignited both academic and practical interest in this issue. It has been argued that fluctuations can be suppressed by anharmonic coupling between bending and stretching modes resulting in robust and stable graphene layers on various substrates.[5] The emergence of "ripples" and "wrinkles" on the scale of ≈ 1 nm – 10 nm in graphene was interpreted by invoking the Mermin-Wagner theorem.[6] Atomistic Monte Carlo simulations predicted the spontaneous formation of *intrinsic ripples* in graphene, with a size distribution peaked ≈8 nm, due to thermal fluctuations.[7] However, a detailed microscopic investigation of graphene on ultra-flat mica substrate revealed the apparent height variation in the graphene layers to be less than 25 picometres, i.e. 25×10^{-12}, indicating the suppression of any existing intrinsic ripples in graphene.[8] It should be noted that when the Mermin-Wagner theorem is applied to a large but finite 2D material system, crystalline order is not prohibited. Short-range order is expected to form even in the thermodynamic limit.[9,10] Although many studies have

J. Teeter, D. Wright, A. A. Balandin
Department of Materials Science and Engineering
University of California
Los Angeles, CA 90095, USA
E-mail: balandin@seas.ucla.edu

J. Teeter, N. Y. Kim, D. Wright, A. Z. Stieg, J. Miao, A. A. Balandin
California NanoSystems Institute
University of California
Los Angeles, CA 90095, USA

N. Y. Kim, J. Miao
Department of Physics and Astronomy
University of California
Los Angeles, CA 90095, USA

T. Debnath, T. Geremew, R. K. Lake
Department of Electrical and Computer Engineering University of California
Riverside, CA 92521, USA

N. Sesing, T. Salguero
Department of Chemistry
University of Georgia
Athens, Georgia 30602, USA

M. Chi
Center for Nanophase Materials Sciences
Oak Ridge National Laboratory
Oak Ridge, Tennessee 37831, USA

A. A. Balandin
Center for Quantum Science and Engineering
University of California
Los Angeles, CA 90095, USA

The ORCID identification number(s) for the author(s) of this article can be found under https://doi.org/10.1002/adma.202409898

DOI: 10.1002/adma.202409898

examined the thermodynamic stability and ripple formation in 2D graphene layers, the stability of van der Waals materials in the atomic chain limit has not been fully addressed.

Van der Waals materials with 1D structural motifs have attracted recent attention.[11–24] These materials include the family of transition metal trichalcogenides with the formula MX_3, e.g. $TaSe_3$, along with other metal chalcogenide compositions such as Nb_2Se_9, metal halides, including $NbCl_4$, and metal chalcohalides, like $(TaSe_4)_2I$. These van der Waals materials have quasi-1D crystalline structures, which results in quasi-1D features in their electronic and phononic properties. Exfoliation routes, including mechanical and solvent-based sonication-assisted actions, cause 1D crystals to exfoliate into ribbons or wire-like structures, by analogy to the exfoliation of 2D materials into 2D sheets. In principle, one expects van der Waals materials, containing 1D motifs, to exfoliate, ultimately, into individual atomic chains with a cross-sectional area on the order of 1 nm × 1 nm. However, the published reports of such exfoliation experiments have yielded bundles of atomic chains with cross-sectional areas of ≈10 nm × 10 nm or larger (see references in the editorial[11]). There have been reports of successful *encapsulation* of individual atomic chains of CrI_3 and Sb_2Se_3 inside single-walled carbon nanotubes (CNTs).[25,26] The interaction of the chains with the CNT wall was essential for their stabilization and significant charge transfer between the 1D chain and CNT was noted. Prior claims of individual atomic chains, either suspended or supported on substrates, have not been entirely conclusive, nor have these reports addressed the issues related to exfoliation energies and stability. Given recent attention to 1D van der Waals materials, questions about the stability of atomic chains derived from 1D solid crystals gain particular significance. It should be noted that 1D van der Waals solid crystals are substantially different from molecular wires, which can also be considered quasi-1D material systems.[27,28] Exfoliating or processing 1D van der Waals materials from bulk crystals to the scale of individual atomic chains would signify a *convergence* of the top-down approach with the bottom-up approach of molecular wire synthesis.

The possibility of reaching the 1D atomic chain limit has practical implications. Nanowires made of 1D van der Waals metals are candidates for future interconnect technologies owing to their high breakdown current densities.[29] Some 1D metals reveal Peierls' phase transitions, with the formation of charge density waves (CDW), and other strongly correlated phenomena.[30–34] The CDW effects discovered in van der Waals materials, including above room temperature (RT), can be exploited to achieve a variety of new device functionalities.[35] Electron transport in ultimately downscaled atomic chains can be controlled with the electric gate bias more efficiently than in the channels with larger diameters.[36,37] Van der Waals materials with 1D motifs in their crystal structure have been tested for utilization as individual device channels and as fillers in composites. Specific examples of the latter include $TaSe_3$ van der Waals nanowires in composites[38] or NbS_3 fillers in printable electronic inks.[39] Chemically exfoliating the fillers to the individual atomic chains or a few-chain bundles with extremely high aspect ratios can bring significant benefits to composite applications. Composites with atomically thin and micrometer-long metallic fillers can achieve percolation threshold at lower filler loading fractions, allow filler alignment, and reveal other unique properties.[40]

There is another interesting aspect to the question of reaching the 1D atomic chain limit. One can consider the van der Waals material to be a *true*-1D if it contains covalent bonds only in the atomic chain and the chains are bound together by typically weak van der Waals forces.[41] The material is *quasi*-1D if it contains strong covalent bonds in the 1D chains, and the chains are bonded by forces beyond weak van der Waals interactions, *e.g.*, weak covalent bonds, ionic electrostatic interactions, or dative-type bonding. According to this delineation, a 1D material like MoI_3 is true-1D because the Mo-I bonds are covalent, intrachain bonds, and the crystal is held together solely by van der Waals interchain interactions (**Figure 1**a). On the other hand, a 1D material like Ta_2Se_8I is quasi-1D due to stronger interchain interactions. Often written as $(TaSe_4)_2I$, this material contains $TaSe_4$ chains with Ta-Se intrachain covalent bonding, and the iodine is present as iodide ions located between chains, with ionic-type electrostatic interactions between the chains and ions (Figure 1b).

In this study, we consider two representative van der Waals materials containing 1D motifs, namely MoI_3, as an example of a *true*-1D material, and $(TaSe_{4)2}I$, as an example of a *quasi*-1D material. Both materials have revealed exotic properties in either the bulk or large-diameter nanowire form, which has provided additional motivations for this study. Specifically, it was suggested that MoI_3 is an antiferromagnetic electrical insulator, and the particular spin texture can be preserved to the limit of individual chains.[42] The quasi-1D $(TaSe_{4)2}I$ is considered a Weyl semimetal with Weyl points located above and below the Fermi level, forming pairs with the opposite chiral charge. At temperatures below the Peierls transition temperature, $(TaSe_4)_2I$ reveals the CDW phase.[43] It has been reported that $(TaSe_4)_2I$ exhibits a correlated topological phase, which arises from the formation of CDW in a Weyl semimetal.[44,45] Both these van der Waals quantum materials represent interesting avenues for exploring the interplay of correlations and topology.

Using the representative 1D van der Waals materials, this work addresses the following questions. Can solid crystals be exfoliated to the individual atomic chains that constitute their structure? Are these atomic chains thermodynamically stable and isolable without encapsulation? Do intrinsic ripples necessarily appear along individual chains of atoms? Can the individual chain limit be achieved for both *true*-1D and *quasi*-1D materials, or do the additional interchain interactions in quasi-1D examples preclude the isolation of their chains? Electron and atomic force microscopies were employed to investigate the presence of individual atomic chains of MoI_3 at RT. The feasibility of "atomic-scale processing" of $(TaSe_4)_2I$ with an electron beam to achieve thinned nanowire regions resulting in suspended atomic chains was also assessed. Both Ab initio calculations and molecular dynamics simulations have been used to address cleavage energies and thermodynamic stability of individual atomic chains of 1D van der Waals crystals. Achieving atomic-scale cross-sections in these two selected materials opens the way for top-down processing of other 1D van der Waals materials. Notably, machine learning studies have suggested the existence of hundreds of true-1D and quasi-1D van der Waals materials – some already synthesized and others remaining predicted.[46,47]

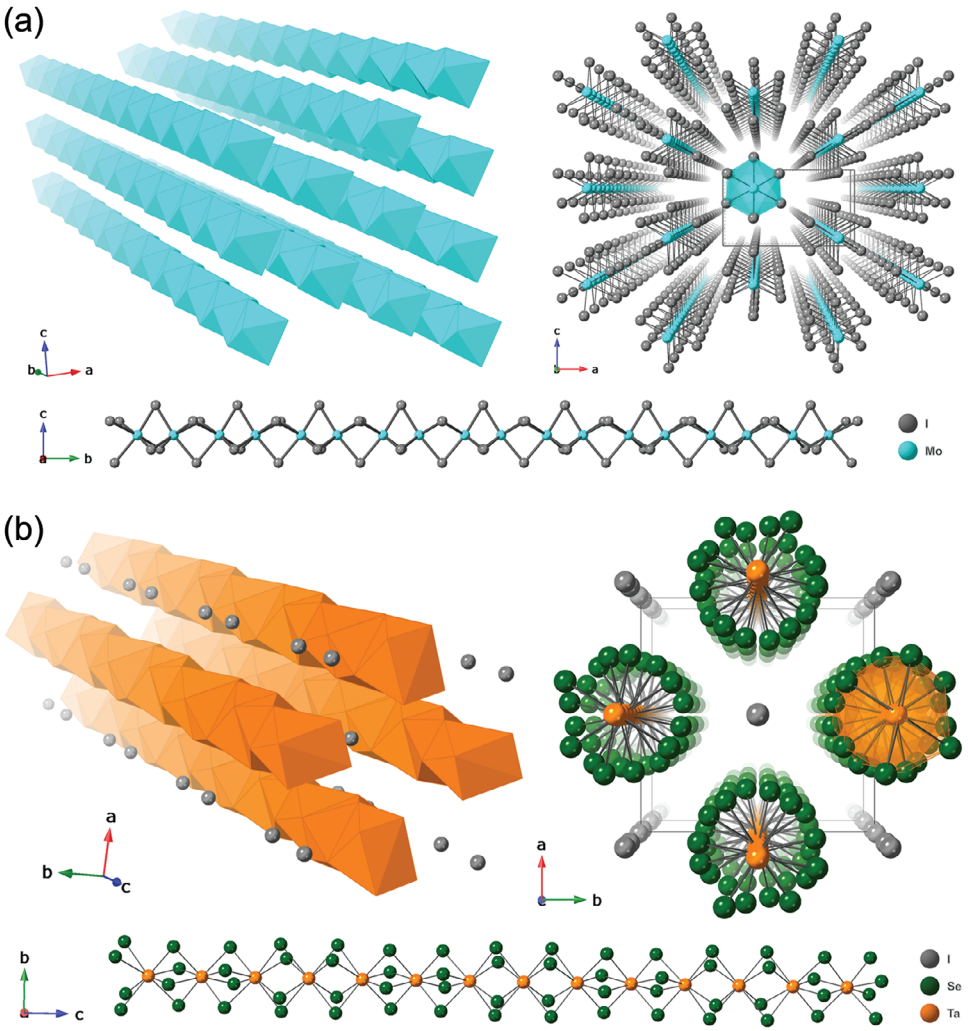

Figure 1. Crystal structures of representative 1D van der Waals materials. a) Angled perspective view of MoI_3 (left, polyhedral representation), view down the *b*-axis (right, ball-and-stick model) with the unit cell outlined in grey, and an individual MoI_3 chain (bottom). b) Angled perspective view of $(TaSe_4)_2I$ (left, polyhedral representation), view down the *c*-axis (right, ball-and-stick model) with the unit cell outlined in grey, and an individual $TaSe_4$ chain (bottom).

2. Results and Discussion

Chemical vapor transport-synthesized (CVT) MoI_3 crystals were exfoliated by liquid-phase exfoliation (LPE) in a mixture of H_2O and isopropanol.[48] LPE processing steps were optimized to provide nanowires with smaller diameters (see experimental section). Exfoliated dispersions were centrifuged to isolate atomic bundles, i.e. nanowires, with smaller cross-sections, and these samples were spin-coated onto substrates or drop-cast onto electron microscopy grids. The distribution of van der Waals nanowire diameters depends strongly on the details of the LPE process. The process was optimized allowing for the exfoliation of nanowires with smaller diameters via an extensive trial-and-error approach. The cross-sectional area of the same batches of exfoliated MoI_3 bundles deposited on various substrates was surveyed using both SEM and AFM. While AFM is known to provide accurate height profiles of nanowire samples, the observable apparent width can be substantially larger due to convolution effects from the AFM tip.[49,50] On the other hand, SEM can give accurate information on the width of the nanowire but does not provide cross-sectional height. Here, several different supporting substrates were used, including mica, which was selected for its atomic flatness to observe features with a height of less than 1 nm in AFM measurements.

SEM and AFM inspection of the same exfoliated nanowires with relatively large diameters was used to establish a typical aspect ratio of the cross-section of these nanowires, where the aspect ratio is expected to depend mainly on the exfoliation energies of 1D materials in directions perpendicular to the nanowire axis. The effect of the substrate on the aspect ratio is expected to be weak for the solvent-based processing as compared to mechanical exfoliation. To determine typical aspect ratios, we started with the nanowires of a relatively large cross-section area. **Figures** 2a,b show the same nanowires imaged with SEM and AFM, respectively. Figure 2c,d present topographic, i.e. height, AFM images acquired at locations indicated in Figure 2b. Relatively small as-

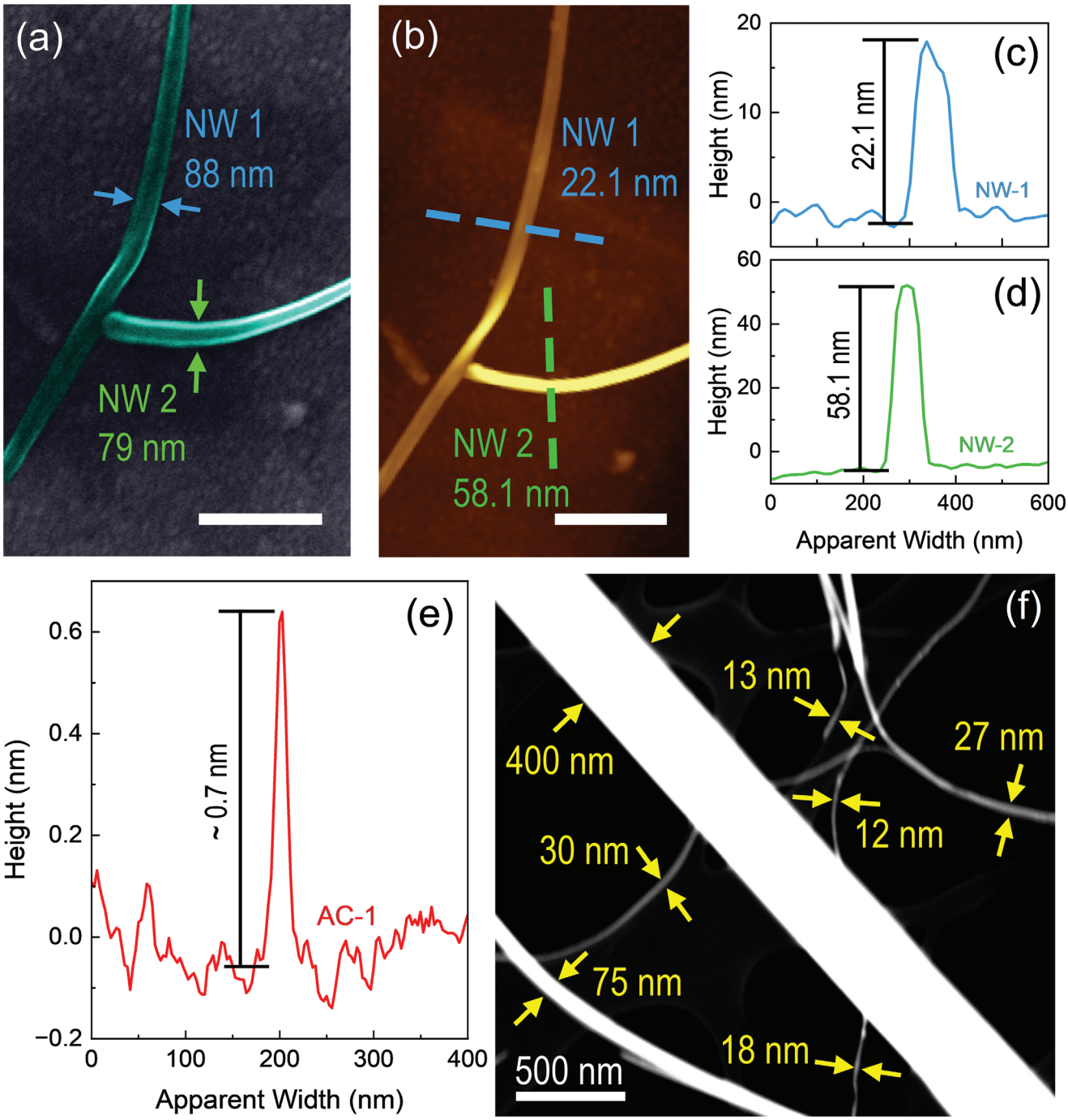

Figure 2. Microscopy images of 1D van der Waals nanowires and atomic chains. a) SEM image of exfoliated MoI_3 nanowires labeled "NW 1" and "NW 2" with indicated widths. b) AFM image of the same nanowires with the indicated scan directions and height. c) AFM height profile of the exfoliated MoI_3 nanowire labeled "NW 1". d) The same for "NW 2". e) The AFM height profile of MoI_3 nanowire on mica substrate with the smallest height of ≈0.7 nm, corresponding to the single atomic chain. The large *apparent* width is due to the limited in-plane resolution convoluted with the AFM tip profile. f) STEM image (HAADF detector) showing typical distribution of MoI_3 nanowires in a liquid-phase exfoliated sample.

pect ratios were observed for a broad range of nanowires, consistent with the calculated exfoliation energies for the two directions perpendicular to the nanowire axis, discussed below. Since the exfoliation energy does not depend on the cross-section, one can assume that the small aspect ratio is maintained for the exfoliated nanowires of small cross-sections. Therefore, in this context, an AFM height of ≈1 nm should be indicative of an individual atomic chain for such materials. Mica has been used previously as an atomically flat substrate, including for the task of examining the number of atomic planes and possible ripples in

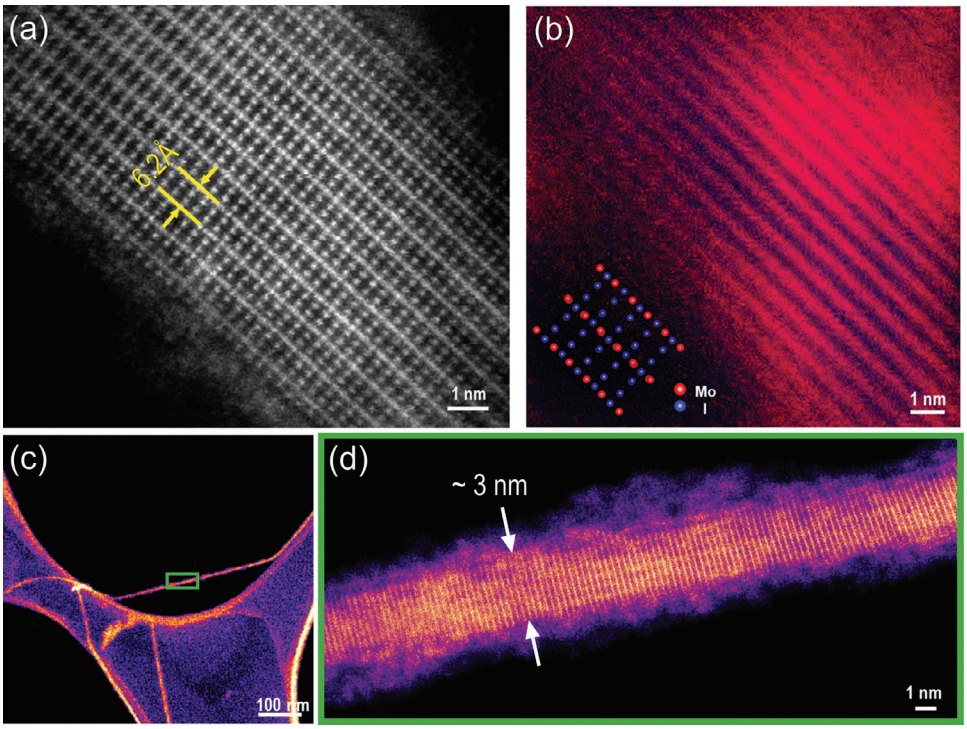

Figure 3. Aberration-corrected STEM images of MoI_3 nanowires. a) Atomically resolved HAADF image of 10 nm wide nanowire with the interatomic distance between the atomic chains of MoI_3 = 6.2 Å. b) STEM-EDS elemental mapping of the same 10 nm wide nanowire. Superimposed EDS images of Mo and I confirm that elemental composition is preserved after exfoliation. The inset shows the atomic arrangement. c) Image of suspended nanowire on lacey carbon grid. d) Close-up of the nanowire with a width of ≈3 nm, which corresponds to about four atomic chains. The chemical residue after exfoliation is seen on the surface of the nanowire.

2D graphene.[8,51] For this reason, it was utilized to locate isolated MoI_3 bundles with the smallest height profile. A representative AFM cross-sectional height profile across an isolated MoI_3 nanowire, shown in Figure 2e, reveals the height of the nanowire (≈0.7 nm) to be consistent with a single atomic chain of MoI_3. The associated AFM image is provided in the Supporting Information (Figure S5, Supporting Information). One should note that solvent-based exfoliation gives nanowires with a wide distribution of cross-section areas. A representative scanning transmission electron microscopy (STEM) image of exfoliated MoI_3 nanowires, illustrating the distribution of the widths is presented in Figure 2f.

Aberration-corrected STEM was used to confirm the crystallinity and stability of the thinnest liquid-phase exfoliated MoI_3 nanowires. These studies allowed for the resolution of distinct Mo and I atomic columns along the [0 0 1] crystallographic direction. **Figure 3a** reveals the atomic structure of a 10-nm-wide MoI_3 nanowire with an observable distance between individual atomic columns of 6.2 Å. A superimposed energy dispersive X-ray spectroscopy (EDS) elemental map differentiates the atomic columns of Mo from those of I (see Figure 3b). Figure 3c-d shows a suspended MoI_3 nanowire with a diameter of 3 nm, demonstrating the structural stability of MoI_3 nanowires with dimensions close to individual atomic chains at RT. The blurry residue on the nanowire surface is the result of contamination during the exfoliation process. The combined AFM and STEM data for exfoliated MoI_3 indicate that the top-down approach of LPE of van der Waals materials can be extended to its ultimate limit of individual atomic chains. The resulting few-chain nanowires preserve their crystallinity and appear to be stable in the single-atomic chain limit at RT.

A second material system grown using the CVT technique, $(TaSe_4)_2I$, was also explored. In addition to LPE, attempts to thin the nanowires down to an individual atomic plane via electron beam exposure were carried out. Small $(TaSe_4)_2I$ crystals were exfoliated into atomic bundles via LPE in a mixture of H_2O and isopropanol solvents. Dispersions were centrifuged and drop-cast onto grids for TEM imaging. A high-resolution TEM image shown in **Figure 4a-b** verifies the crystallinity of the $(TaSe_4)_2I$, nanowires after LPE processing. The distance between the columns of atoms is 6.93 Å, nearly identical to the distance between Ta atoms in adjacent $TaSe_4$ chains as seen in the crystal structure of $(TaSe_4)_2I$.[52] This 21 nm-wide nanowire contains approximately thirty individual chains. The atomic-chain limit in $(TaSe_4)_2I$ is different than in MoI_3 due to the presence of interchain iodide ions (Figure 1b). Prior studies have noted an iodine deficiency in $(TaSe_4)_2I$, therefore it is not clear whether a few or a single chain $(TaSe_4)_2I$ will include all formally associated iodide ions.

By adjusting the electron beam acceleration voltage and dosage, we determined the exposure parameters that allowed us to thin down the $(TaSe_4)_2I$ nanowires to atomic scale (see **Figure 5a-d**). Processed nanowires exhibited structural non-uniformity, although regions of uniform diameter were also observable. Figure 4a-d shows representative TEM images highlighting the evolution of suspended $(TaSe_4)_2I$ nanowires under

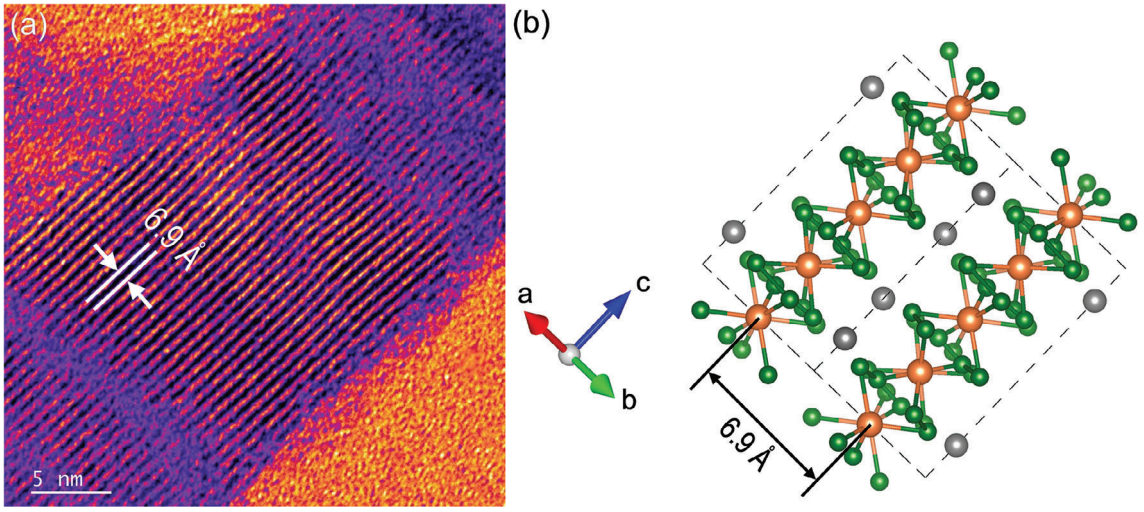

Figure 4. High-resolution TEM imaging of $(TaSe_4)_2I$ nanowires. a) Image of an as-prepared $(TaSe_4)_2I$ nanowire before electron beam processing showing a nanowire with a diameter of 21 nm on a 100-nm thick SiN window. b) Corresponding schematic of the crystal structure.

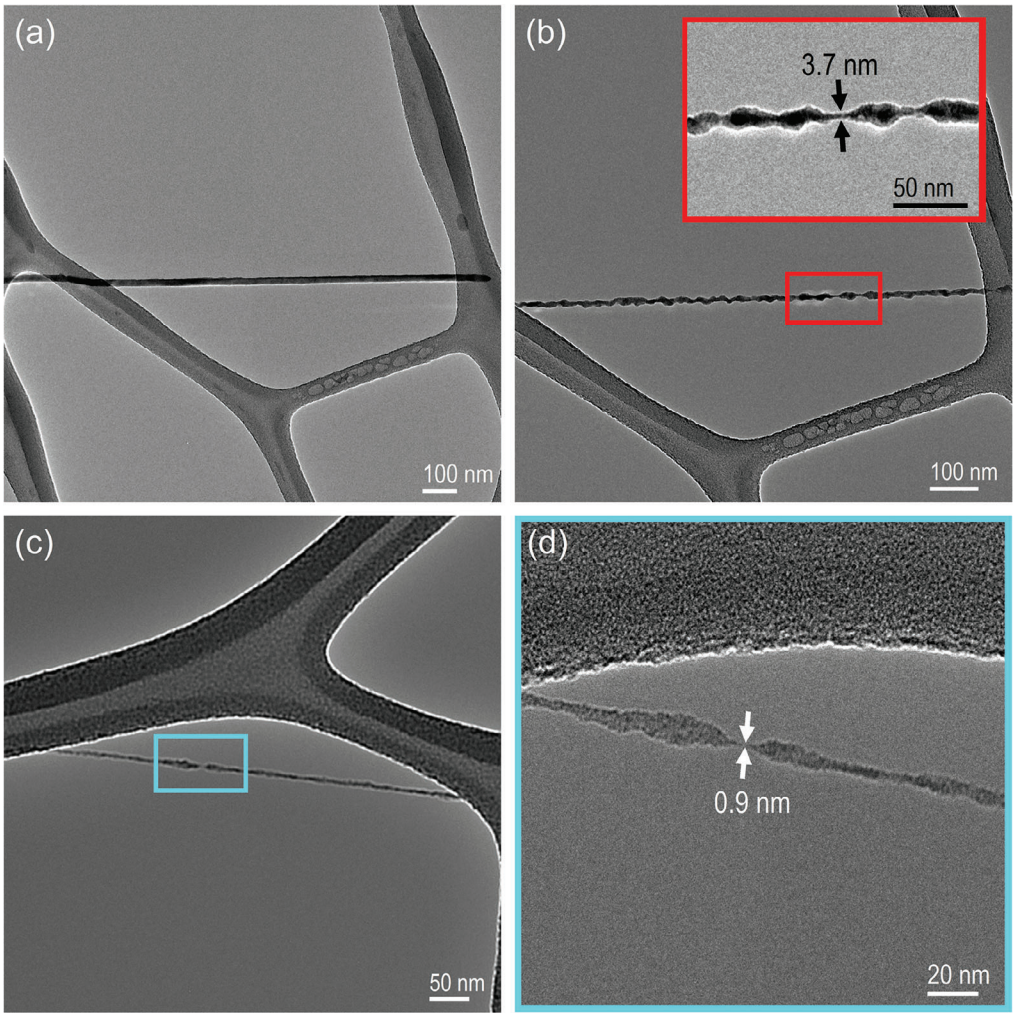

Figure 5. Electron-beam processing of $(TaSe_4)_2I$ nanowires. a) A 22.7-nm diameter nanowire, imaged with TEM under 120 kV accelerating voltage. b) The same nanowire is shown after 2 min of exposure to the electron beam along with a thin section of the nanowire with a diameter of 3.7 nm (inset). c) Electron beam processing on an initially much thinner wire. d) The narrow section of a nanowire with a diameter of ≈0.9 nm, corresponds to an individual atomic chain.

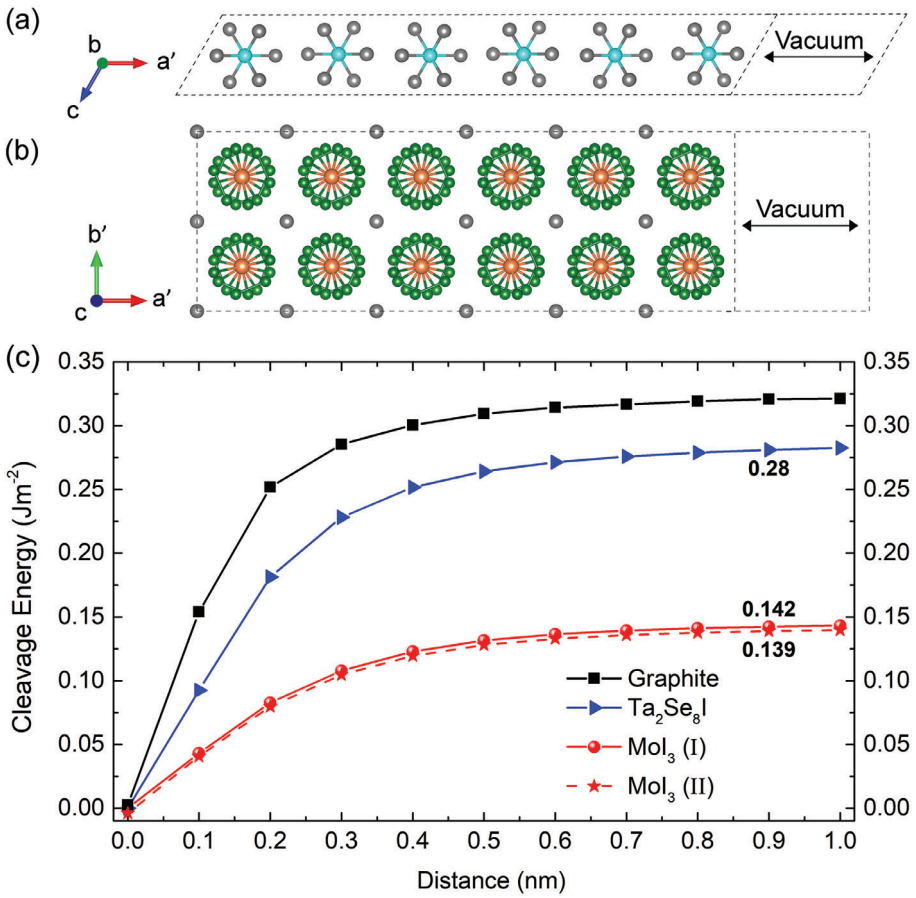

Figure 6. a) MoI_3 and b) $(TaSe_4)_2I$ slab structures for calculating the exfoliation energies. The rotated lattice constants indicated with a prime, are defined in the SM. c) Cleavage energy as a function of vacuum layer distances for MoI_3 and $(TaSe_4)_2I$. The red curves represent the energy of MoI_3 cleaved through two van der Waals gaps (001 and 100 plane) while the blue line shows the energy of $(TaSe_4)_2I$ which is same in either van der Waals direction. For comparison, the cleavage energy of graphite is also shown.[55] The energies at 0.9 nm vacuum separation are reported as the cleavage energy values in this work.

electron beam exposure. The nanowire diameter of 22.7 nm (see Figure 5a) was reduced to 3.7 nm (see Figure 5b) in ≈2 min. Further beam exposure resulted in the continuous removal of atomic layers until the nanowire became too thin and snapped. Electron-beam processing of thinner nanowires produced atomically thin sections, i.e. individual atomic chains. A nanowire with a diameter of ≈7 nm was exposed to the electron beam at a dose rate of 41 e Å^{-2} s^{-1} for a duration of ≈2 min. The resulting nanowire structure shown in Figure 5c demonstrates a segment of ≈0.9 nm diameter, which represents an individual atomic chain. The continuous atomic chain is seen in Figure 5d. It is important to note that the stoichiometry of the atomic chain may change as a result of electron beam-induced thinning due to the loss of iodine atoms. If the iodine atoms were lost, these results suggest that the suspended Ta_2Se_8 structure is also thermodynamically stable. The latter is confirmed by the computations discussed below. It is also possible that contaminants, i.e. carbon atoms, may play a role in the thinning process. One cannot examine in detail the composition of the resulting chains due to a limitation on the time of the electron beam exposure required to get to the atomic chain limit. The key takeaway from these experiments is that one can readily and controllably "manufacture" individual atomic chains of solid crystal material that remain stable at RT.

3. Theoretical

To rationalize the experimental observations and to provide additional support to the possibility of exfoliation and processing of 1D van der Waals crystals to individual atomic chains, density functional theory (DFT) studies of MoI_3 and $(TaSe_4)_2I$ were conducted. After initial structural optimization of the bulk structures, the exfoliation, i.e. cleavage, energies for these materials were calculated. As the next step, we performed structural optimization of the individual chains and determined the stability of the chains by calculating their phonon dispersions and carrying out finite temperature Ab initio molecular dynamics calculations. The details of the DFT and phonon dispersion calculations are provided in the METHODS section while the details of the exfoliation energy calculations are provided in the Supporting Information.

The exfoliation energy for each direction of 1D material is defined as the energy required to separate a 2D layer from the bulk material. It is calculated by taking the energy difference of

Table 1. Cleavage Energy for 1D and 2D van der Waals Materials.

Material	Energy	Method	Refs.
MoI_3	0.142 Jm^{-2}, 0.139 Jm^{-2}	DFT	This work
$(TaSe_4)_2I$	0.280 Jm^{-2}	DFT	This work
$GeSe_2$	0.05 Jm^{-2}	DFT	[56]
Graphene	0.34 Jm^{-2}	Experimental	[53]
Graphite	0.37 Jm^{-2}	Experimental, DFT	[54]
GeP_3	1.14 Jm^{-2}	DFT	[57]
GeS	0.52 Jm^{-2}	DFT	[58]
NaSnP	0.81 Jm^{-2}	DFT	[59]
MoS_2	0.6 Jm^{-2}	Experimental	[60]
$CrSbSe_3$	0.49 Jm^{-2}	DFT	[61]

a bulk supercell, E_B, and its corresponding 2D slab, E_{2D}, created by adding a vacuum layer to the supercell. To represent the bulk structure we used a supercell, which is periodic in all directions. The 2D slabs were formed by adding a vacuum layer along one axis of the supercell while keeping the original periodic conditions along the other two axes. This creates a slab with a left and right surface as shown in **Figure 6**a,b. The energy difference of the bulk and slab structures divided by the surface area of the two surfaces, $2S$, gives the exfoliation or cleavage energy of that material, *i.e.* $E_c = (E_{2D} - E_B)/(2S)$. The schematics of the supercells and details of the calculations are provided in the Supplementary Materials. We increased the size of the vacuum layer until the change in exfoliation energy became negligible. Figure 6c shows the exfoliation energy curves for MoI_3 and $(TaSe_4)_2I$ as a function of vacuum distances. For MoI_3, the exfoliation energies along the two directions perpendicular to the nanowire were determined to be 0.142 J m^{-2} and 0.139 J m^{-2}, and for $(TaSe_4)_2I$, the exfoliation energy was found to be 0.280 J m^{-2}, for both directions perpendicular to the nanowire. For comparison, the exfoliation energy for graphite is 0.32–0.37 J m^{-2}.[53–55] Our calculations indicate that both materials have a lower cleavage energy than graphite and hence can be easily cleaved or exfoliated, which agrees with our experiments. The resulting nanowires should also have aspect ratios close to unity, and the experimental TEM width or AFM height of ≈1 nm is a good indicator of individual atomic chains. To place our results in the general context of van der Waals materials, we summarized the exfoliation energies for several important van der Waals materials in **Table 1**.

To determine the stability of each atomic chain, we first relaxed the chain structures. The relaxed $(MoI_3)_2$ chains were dimerized as they were in the bulk, and the Mo-Mo distances changed little from their bulk values. For the Ta_2Se_8 chains, we took a single symmetric chain from the bulk unit cell consisting of 4 Ta atoms and 16 Se atoms, i.e. $(TaSe_4)_4$, with a uniform Ta-Ta distance of 3.222 Å. We have not included iodine atoms since the iodine atoms are loosely bonded between the $(TaSe_4)_4$ chains and were expected to be lost or act as random adsorbates after the electron beam processing. After relaxation, the chain dimerized with alternating long (3.452 Å) and short bonds (2.991 Å) between the Ta atoms. The fact that we observed dimerization instead of tetramerization[62,63] maybe an artifact of the cell size used for the relaxation. For the MD calculations, we doubled the primitive cells as shown in **Figure 7**a,c, i.e. $(MoI_3)_4$ and $(TaSe_4)_8$. After 2000 fs at $T = 200$ K, we did see what appeared to be tetramerization in the $(TaSe_4)_8$ chain. The Ta-Ta bond distances followed the pattern S-L-S-M where S = 3.0 Å, L = 3.5 Å, and M = 3.4 Å. At 300 K, there were still vestiges of the tetramerization, but with greater variation among the bond lengths. The main result from the MD calculations was that at $T = 300$ K after 2000 fs of simulation time, the individual chains of $(MoI_3)_4$ and $(TaSe_4)_8$ remained intact, indicating that the individual chains were stable at RT. This is again in line with our experimental observations.

As another check of stability, we calculated the phonon dispersions of the individual chains shown in Figure 7b,d. The lack of negative branches is a further indication of the stability of the individual chains. The small negative frequencies, near the Γ point, were attributed to numerical error and can likely be removed by using larger supercells. Thus, both the calculated phonon dispersions and the MD calculations indicate that single chains of MoI_3 and $TaSe_4$ are thermodynamically stable at RT. The results of the calculations support our conclusions that 1D atomic chains are stable and can be obtained by exfoliation or electron-beam processing. The encasing of 1D atomic chains inside CNTs or other structures was not required to maintain the stability of the examined materials.

4. Conclusions

We achieved the 1D-chain limit by two methods, exfoliation and electron-beam processing, and proved the thermodynamic stability by two theoretical methods. The results were discussed in the context of the Mermin–Wagner theorem. We have utilized two representative layered materials with 1D motifs in their crystal structure, namely MoI_3, and $(TaSe_4)_2I$. The detailed HR-TEM and AFM studies confirmed the presence of stable individual atomic chains of MoI_3 at RT. We also demonstrated that 1D van der Waals materials with low exfoliation energy, such as $(TaSe_4)_2I$, can be processed with an electron beam to achieve suspended individual atomic chains. We did not observe "intrinsic ripples" in the exfoliated nanowires of these materials when examining them on ultra-flat mica substrates. The *ab initio* calculations corroborated our conclusions regarding the low cleavage energies and the thermodynamic stability of individual atomic chains in such 1D van der Waals materials. The calculated exfoliation energies along the two directions perpendicular to the nanowire are ≈0.14 J m^{-2} and 0.28 J m^{-2} for MoI_3 and $(TaSe_4)_2I$, respectively, which are factors of 2.6 and 1.3 smaller than that of graphite. Our results indicate that the top-down approach in material processing can be extended to the scale of the atomic chains, which is important for the electronic application of these 1D quantum materials.

5. Experimental Section

Material Synthesis: MoI_3 and Ta_2Se_8I crystals were prepared by the chemical vapor transport method using the previously reported conditions. Structure and composition were confirmed by PXRD and SEM-EDS, respectively.

Liquid Phase Exfoliation of MoI_3: Following previous studies on 2D TMDs, a combination of solvents permits tunability of dispersive components for optimal dispersion of nanowires. The solvents used for our experiment were H_2O and isopropanol. The percentage of isopropanol by volume was varied to get a broad range of solubility parameters. 10 mL of

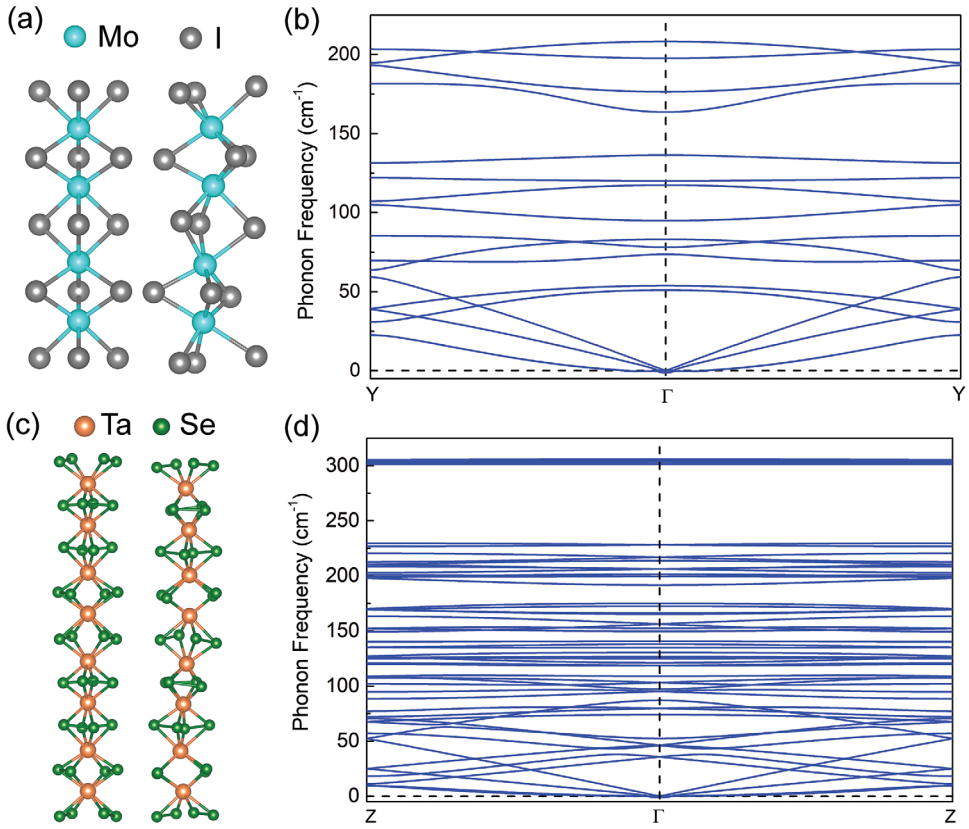

Figure 7. Computational stability analysis. a) MD calculations of a single-chain $(MoI_3)_4$ before (left) and after (right) 2000 fs at 300 K. b) The single-chain phonon dispersion of $(MoI_3)_2$ plotted along the chain direction. c) MD calculations of a single-chain $(TaSe_4)_8$ structure before (left) and after (right) 2000 fs at 300 K. d) The single-chain phonon dispersion of $(TaSe_4)_4$ structure plotted along the chain direction.

mixed isopropanol and H_2O solvent was added to 1 mg of as-synthesized bulk MoI_3 in a 20 mL glass vial. Probe sonication (Fisher Scientific, FB-705) was performed by introducing a 1/8″ diameter probe, into solution with a 2 s/2 s on/off cycle at an amplitude of 20 for 10 min. The dispersions were sealed and placed into a bath sonicator (Branson 2800) with a fixed frequency of 40 kHz for 1 h to disperse the nanowires further. 5 mL of dispersion was extracted from each sample and centrifuged (Eppendorf centrifuge 5810) at 3000 rpm for 20 min to isolate the large aggregations from the thinner material. Approximately 2 mL of supernatant solution was extracted and used for further analysis. For MoI_3 a ratio of 50% isopropanol by volume was selected based on the dark color (see Supporting information for details). A strong Tyndall effect after centrifugation indicated a good dispersion.[64,65]

Liquid Phase Exfoliation of Ta_2Se_8I: 20 mL of mixed isopropanol and H_2O solvent were added to 10 mg of as-synthesized Ta_2Se_8I in a 20 mL glass vial. The vial was placed into a bath sonicator (Branson 2800) with a fixed frequency of 40 kHz for 9 h. 10 mL of solvent was extracted and centrifuged at 2000 rpm for 40 min (Eppendorf centrifuge 5810). 5 mL of supernatant was collected and then centrifuged again at 2000 rpm for 20 min. Approximately 2 mL of the final supernatant was extracted and used for further analysis. For $(TaSe_4)_2I$ a ratio of 20% isopropanol by volume was selected. The optimum mixes and sonication conditions for higher concentrations of nanowires with a small cross-section were found after extensive testing.

SEM and AFM Inspection: For cross-sectional analysis, 1 µL of the final MoI_3 supernatant was spin-coated onto electron beam evaporated gold substrates and freshly cleaved V-1 mica from SPI at 1000 rpm for 30 s. High-density regions of thin nanowires were present around evaporation rings, visible on an optical microscope. The SEM (Zeiss Supra VP40) at an accelerating voltage of 20kV was used to measure quantitative widths of exfoliated MoI_3 nanowires. In-lens electron detection at a 3 mm working distance provided sharp contrast images of MoI_3 nanowires. To minimize AFM tip convolution effects, a Bruker tip (Scanasyst-air-HPI) with small tip radius ≈2 nm was used. The landing and scanning parameters were modified for maximum preservation of the probe tip during scanning. The width deconvolution of AFM data was done using a method, for the ideal case of an object with a circular cross-section object on a perfectly flat surface in a contact mode.[66]

Low-kV STEM Imaging: 2.8 mg of mm-scale CVT-grown MoI_3 crystals were added to a 50 mL centrifuge tube, along with 14 mL of ultrapure water and 6 mL electronics grade isopropanol. This material was probe sonicated with ice bath cooling for 1.5 h at 30 Amp, followed by 2.5 h of bath sonication. The resultant product was a homogenous dark brown suspension. Exfoliated samples were drop-cast immediately after sonication onto individual lacey carbon TEM grids and allowed to dry under ambient conditions. STEM imaging was performed using a Hitachi SU9000EA microscope with a 20kV accelerating voltage.

Aberration Corrected STEM: An aberration-corrected STEM (JEOL JEM-ARM200F NeoARM), operating at 200 KV was used. This microscope was equipped with an advanced Cs corrector (ASCOR) and an energy-dispersive X-ray spectroscopy (EDS) system, which includes dual silicon-drift detectors. This configuration enabled comprehensive STEM imaging and concurrent EDS mapping analysis. Each EDS elemental map image was processed using a Wiener filter to reduce noise. The MoI_3 samples were prepared by drop-casting on a lacey carbon TEM grid and then dried at ambient temperatures to prevent heat-induced transformations. This drying method retains solution residues, which can be observed adhering to the MoI_3 chains. An Ultra-STEM 100 was used to

minimize structural transformations induced by the electron beam, operating at 60 KV.

TEM Electron-Beam Processing: TEM (FEI Tecnai 12) operating at 120 kV was used for processing of $(TaSe_4)_2I$. The Ta_2Se_8I nanowire samples were prepared by drop-casting the dispersion onto a lacey carbon TEM grid and subsequently dried at ambient temperatures to prevent heat-induced transformations. Wires were first surveyed at low electron dosage rates and high spot sizes. Once a suitable wire was found, the spot size was reduced, and the dose rate increased. Electron beam processing begins taking place at the edges of the material. The process starts immediately after decreasing the spot size and the material erodes into a non-uniform structure. Atomically thin regions are present along smaller wires after approximately 1 min of electron-beam exposure.

DFT Calculations: Structural optimization and other calculations were carried out using the projector augmented-wave (PAW) pseudopotentials[67] and Perdew-Burke-Ernzerhof (PBE) exchange-correlation functionals,[68] as implemented in VASP.[69,70] The van der Waals interactions were included by the semi-empirical correction of Grimme-D3.[71] For all calculations, the cutoff energy for the plane wave basis was chosen to be 520 eV. For the bulk relaxations, converged k-point grids of 6×12×12 and 8×8×7 were used for MoI3 and $(TaSe_4)_2I$, respectively. For the chain relaxations, converged k-point grids of 1×20×1 and 1×1×10 were used for $(MoI_3)_2$ and $(TaSe_4)_4$, respectively. All structures were relaxed until the forces on each atom were less than 10^{-5} eV $Å^{-1}$ and the energy convergence reached 10^{-9} eV. The chains of $(MoI_3)_2$ and $(TaSe_4)_4$ lie along the ***b*** and ***c*** axes, respectively, and in single chain structures, they are surrounded by a 10 Å vacuum in the other two directions. The phonon dispersions were calculated using the finite difference approach as implemented in Phonopy[72] with supercell sizes of 1×4×1 (MoI_3) and 1×1×4 $(TaSe_4)_4$. Ab initio MD calculations, as implemented in VASP, used a canonical ensemble and Nose-Hoover thermostat with a time step of 1 fs, for a total of 2000 fs.

Supporting Information

Supporting Information is available from the Wiley Online Library or from the author.

Acknowledgements

A.A.B. acknowledges the support of the Vannevar Bush Faculty Fellowship (VBFF) under the Office of Naval Research (ONR) contract N00014-1-1-2947 and prior support from the National ScienceFoundation (NSF) DMR- 1921958. The work at UCR and the University of Georgia was supported, in part, via the subcontracts of the ONR project N00014-21-1-2947. N.Y.K. and J.M. acknowledge support from the US Department of Energy (DOE), Office of Science, Basic Energy Sciences (BES), Division of Materials Sciences and Engineering under award DE-SC0010378. M. C. acknowledges the Early Career Research Program supported by the DOE, Office of Science, Basic Energy Sciences (BES). The AFM, SEM, and TEM studies were performed at the UCLA California NanoSystems Institute (CNSI). The STEM imaging and analysis were conducted at the Center for Nanophase Materials Sciences (CNMS) at the Oak Ridge National Laboratory (ORNL). This work used STAMPEDE3 at TACC through allocation DMR130081 from the Advanced Cyberinfrastructure Coordination Ecosystem: Services & Support (ACCESS) program,[73] which was supported by NSF Grants No. 2138259, 2138286, 2138307, 2137603, and 2138296.

Conflict of Interest

The authors declare no conflict of interest.

Author Contributions

A.A.B. conceived the idea, coordinated the project, contributed to experimental data analysis, and led the manuscript preparations. J.T. performed chemical exfoliation, TEM imaging and electron-beam processing, AFM characterization, and contributed to data analyses; T.G. and D.W. contributed to exfoliation and AFM studies. N.S. synthesized bulk crystals using the CVT method and performed some TEM studies. A.S. assisted with AFM studies; N.Y.K., M.C., and J.M. performed STEM studies and contributed to the microscopy data analysis. T.D. and R.K.L. performed DFT and MD simulations. T.S. supervised material synthesis and contributed to data analysis. All authors participated in the manuscript preparation.

Data Availability Statement

The data that support the findings of this study are available from the corresponding author upon reasonable request.

Keywords

1D materials, atomic chains, van der Waals materials

Received: July 9, 2024
Revised: September 22, 2024
Published online:

[1] R. Peierls, *Annales del l'I.H.P.* **1935**, *5*, 177.
[2] L. D. Landau, *Phys. Z. Sowjetunion* **1937**, *11*, 26.
[3] N. D. Mermint, *Phys. Rev.* **1968**, *176*, 250.
[4] N. D. Mermin, H. Wagner, *Phys. Rev. Lett.* **1966**, *17*, 1133.
[5] A. K. Geim, K. S. Novoselov, *Nat. Mater.* **2007**, *6*, 183.
[6] J. C. Meyer, A. K. Geim, M. I. Katsnelson, K. S. Novoselov, T. J. Booth, S. Roth, *Nature* **2007**, *446*, 60.
[7] A. Fasolino, J. H. Los, M. I. Katsnelson, *Nat. Mater.* **2007**, *6*, 858.
[8] C. H. Lui, L. Liu, K. F. Mak, G. W. Flynn, T. F. Heinz, *Nature* **2009**, *462*, 339.
[9] G. Piacente, I. V. Schweigert, J. J. Betouras, F. M. Peeters, *Phys Rev B Condens Matter Mater Phys* **2004**, *69*, 045324.
[10] M. V. Fischetti, W. G. Vandenberghe, *Phys. Rev. B* **2016**, *93*, 155413.
[11] A. A. Balandin, R. K. Lake, T. T. Salguero, *Appl. Phys. Lett.* **2022**, *121*, 040401.
[12] Y. Fang, K. Yang, E. Zhang, S. Liu, Z. Jia, Y. Zhang, H. Wu, F. Xiu, F. Huang, *Adv. Mater.* **2022**, *34*, 2200145.
[13] T. Pham, K. Reidy, J. D. Thomsen, B. Wang, N. Deshmukh, M. A. Filler, F. M. Ross, *Adv. Mater.* **2024**, *36*, 2309360.
[14] D. L. M. Cordova, Y. Zhou, G. M. Milligan, L. Cheng, T. Kerr, J. Ziller, R. Wu, M. Q. Arguilla, *Adv. Mater.* **2024**, *36*, 2312597.
[15] Z. E. Nataj, F. Kargar, S. Krylyuk, T. Debnath, M. Taheri, S. Ghosh, H. Zhang, A. V. Davydov, R. K. Lake, A. A. Balandin, *J. Raman Spectrosc.* **2024**, *55*, 695.
[16] S. Ghosh, S. Rumyantsev, A. A. Balandin, *Appl. Phys. Rev.* **2024**, *11*, 021405.
[17] C. Cignarella, D. Campi, N. Marzari, Searching for the thinnest metallic wire, arXiv:2312.16968, **2024**.
[18] B. J. Jeong, B. Lee, K. H. Choi, D. Sung, S. Ghods, J. Lee, J. Jeon, S. Cho, S. H. Lee, B. J. Kim, S. Il Kim, J. Huh, H. K. Yu, J. H. Lee, J. Y. Choi, *Nano Lett.* **2023**, *23*, 6269.
[19] A. Poltarak, P. Poltarak, A. Enyashin, V. Komarov, S. Artemkina, V. Fedorov, *Inorg. Chem.* **2022**, *61*, 2783.
[20] S. Baraghani, J. Abourahma, Z. Barani, A. Mohammadzadeh, S. Sudhindra, A. Lipatov, A. Sinitskii, F. Kargar, A. A. Balandin, *ACS Appl. Mater. Interfaces* **2021**, *13*, 47033.
[21] B. J. Kim, B. J. Jeong, S. Oh, S. Chae, K. H. Choi, T. Nasir, S. H. Lee, K. W. Kim, H. K. Lim, I. J. Choi, L. Chi, S. H. Hyun, H. K. Yu, J. H. Lee, J. Y. Choi, *RSC. Adv.* **2018**, *8*, 37724.

[22] G. Liu, S. Rumyantsev, M. A. Bloodgood, T. T. Salguero, M. Shur, A. A. Balandin, *Nano Lett.* **2017**, *17*, 377.
[23] S. Oh, S. Chae, B. J. Kim, A. J. Siddiqa, K. H. Choi, W.-S. Jang, K. H. Lee, H. Y. Kim, D. K. Lee, Y.-M. Kim, H. K. Yu, J.-Y. Choi, *physica status solidi (RRL) – Rapid Research Letters* **2018**, *12*, 1800451.
[24] B. J. Jeong, K. H. Choi, J. Jeon, S. O. Yoon, Y. K. Chung, D. Sung, S. Chae, B. J. Kim, S. Oh, S. H. Lee, C. Woo, T. Y. Kim, J. Ahn, J.-H. Lee, J. Huh, H. K. Yu, J.-Y. Choi, *Adv. Funct. Mater.* **2022**, *32*, 2108104.
[25] Y. Lee, Y. W. Choi, K. Lee, C. Song, P. Ercius, M. L. Cohen, K. Kim, A. Zettl, *Adv. Mater.* **2023**, *35*, 2307942.
[26] G. M. Milligan, Z. F. Yao, D. L. M. Cordova, B. Tong, M. Q. Arguilla, *Chem. Mater.* **2024**, *36*, 730.
[27] L. Li, C. Nuckolls, L. Venkataraman, *J. Phys. Chem. Lett.* **2023**, *14*, 5141.
[28] L. Li, J. Z. Low, J. Wilhelm, G. Liao, S. Gunasekaran, C. R. Prindle, R. L. Starr, D. Golze, C. Nuckolls, M. L. Steigerwald, F. Evers, L. M. Campos, X. Yin, L. Venkataraman, *Nat. Chem.* **2022**, *14*, 1061.
[29] M. A. Stolyarov, G. Liu, M. A. Bloodgood, E. Aytan, C. Jiang, R. Samnakay, T. T. Salguero, D. L. Nika, S. L. Rumyantsev, M. S. Shur, K. N. Bozhilov, A. A. Balandin, *Nanoscale* **2016**, *8*, 15774.
[30] G. Gruner, The Dynamics of Charge-Density Waves **1988**.
[31] S. V. Zaitsev-Zotov, *Physics-Uspekhi* **2004**, *47*, 533.
[32] P. Monceau, *Adv. Phys.* **2012**, *61*, 325.
[33] A. A. Balandin, S. V. Zaitsev-Zotov, G. Grüner, *Appl. Phys. Lett.* **2021**, *119*, 170401.
[34] Z. Barani, T. Geremew, M. Stokey, N. Sesing, M. Taheri, M. J. Hilfiker, F. Kargar, M. Schubert, T. T. Salguero, A. A. Balandin, *Adv. Mater.* **2023**, *35*, 2209708.
[35] S. G. Zybtsev, V. Y. Pokrovskii, V. F. Nasretdinova, S. V. Zaitsev-Zotov, *Physica B Condens Matter* **2012**, *407*, 1696.
[36] T. L. Adelman, S. V. Zaitsev-Zotov, R. E. Thorne, *Phys Rev Lett.* **1995**, *74*, 5264.
[37] Y. Meng, W. Wang, J. C. Ho, *ACS Nano* **2022**, *16*, 13314.
[38] Z. Barani, F. Kargar, Y. Ghafouri, S. Ghosh, K. Godziszewski, S. Baraghani, Y. Yashchyshyn, G. Cywiński, S. Rumyantsev, T. T. Salguero, A. A. Balandin, *Adv. Mater.* **2021**, *33*, 2007286.
[39] T. Geremew, M. Taheri, N. Sesing, S. Ghosh, F. Kargar, T. T. Salguero, A. A. Balandin, *ACS Appl. Electron. Mater.* **2024**, *6*, 4653.
[40] Z. Barani, F. Kargar, Y. Ghafouri, S. Baraghani, S. Sudhindra, A. Mohammadzadeh, T. T. Salguero, A. A. Balandin, *ACS Appl. Mater. Interfaces* **2021**, *13*, 21527.
[41] A. A. Balandin, F. Kargar, T. T. Salguero, R. K. Lake, *Mater. Today* **2022**, *55*, 74.
[42] F. Kargar, Z. Barani, N. R. Sesing, T. T. Mai, T. Debnath, H. Zhang, Y. Liu, Y. Zhu, S. Ghosh, A. J. Biacchi, F. H. Da Jornada, L. Bartels, T. Adel, A. R. Hight Walker, A. V. Davydov, T. T. Salguero, R. K. Lake, A. A. Balandin, *Appl. Phys. Lett.* **2022**, *121*, 221901.
[43] S. van Smaalen, E. J. Lam, J. Lüdecke, *J. Phys.: Condens. Matter* **2001**, *13*, 9923.
[44] W. Shi, B. J. Wieder, H. L. Meyerheim, Y. Sun, Y. Zhang, Y. Li, L. Shen, Y. Qi, L. Yang, J. Jena, P. Werner, K. Koepernik, S. Parkin, Y. Chen, C. Felser, B. A. Bernevig, Z. Wang, *Nat. Phys.* **2021**, *17*, 381.
[45] S. Ghosh, F. Kargar, N. R. Sesing, Z. Barani, T. T. Salguero, D. Yan, S. Rumyantsev, A. A. Balandin, *Adv. Electron. Mater.* **2023**, *9*, 2200860.
[46] G. Cheon, K. A. N. Duerloo, A. D. Sendek, C. Porter, Y. Chen, E. J. Reed, *Nano Lett.* **2017**, *17*, 1915.
[47] Y. Zhu, E. R. Antoniuk, D. Wright, F. Kargar, N. Sesing, A. D. Sendek, T. T. Salguero, L. Bartels, A. A. Balandin, E. J. Reed, F. H. da Jornada, *J. Phys. Chem. C* **2023**, *127*, 21675.
[48] K. G. Zhou, N. N. Mao, H. X. Wang, Y. Peng, H. L. Zhang, *Angewandte Chemie – International Edition* **2011**, *50*, 10839.
[49] J. Shen, D. Zhang, F. H. Zhang, Y. Gan, *Appl. Surf. Sci.* **2017**, *422*, 482.
[50] J. Canet-Ferrer, E. Coronado, A. Forment-Aliaga, E. Pinilla-Cienfuegos, *Nanotechnology* **2014**, *25*, 395703.
[51] W. De Poel, S. Pintea, J. Drnec, F. Carla, R. Felici, P. Mulder, J. A. A. W. Elemans, W. J. P. Van Enckevort, A. E. Rowan, E. Vlieg, *Surf. Sci.* **2014**, *619*, 19.
[52] P. Gressier, L. Guemas, A. Meerschaut, *Acta Crystallographica Section B* **1982**, *38*, 2877.
[53] R. Zacharia, H. Ulbricht, T. Hertel, *Phys Rev B Condens Matter Mater Phys* **2004**, *69*, 155406.
[54] W. Wang, S. Dai, X. Li, J. Yang, D. J. Srolovitz, Q. Zheng, *Nat. Commun.* **2015**, *6*, 7853.
[55] N. S. Vorobeva, A. Lipatov, A. Torres, J. Dai, J. Abourahma, D. Le, A. Dhingra, S. J. Gilbert, P. V. Galiy, T. M. Nenchuk, D. S. Muratov, T. S. Rahman, X. C. Zeng, P. A. Dowben, A. Sinitskii, *Adv. Funct. Mater.* **2021**, *31*, 2106459.
[56] Y. Yang, S. C. Liu, W. Yang, Z. Li, Y. Wang, X. Wang, S. Zhang, Y. Zhang, M. Long, G. Zhang, D. J. Xue, J. S. Hu, L. J. Wan, *J. Am. Chem. Soc.* **2018**, *140*, 4150.
[57] Y. Jing, Y. Ma, Y. Li, T. Heine, *Nano Lett.* **2017**, *17*, 1833.
[58] F. Li, X. Liu, Y. Wang, Y. Li, *J Mater Chem C Mater* **2016**, *4*, 2155.
[59] Y. Jiao, F. Ma, G. Gao, J. Bell, T. Frauenheim, A. Du, *J. Phys. Chem. Lett.* **2015**, *6*, 2682.
[60] B. Rasche, J. Brunner, T. Schramm, M. P. Ghimire, U. Nitzsche, B. Büchner, R. Giraud, M. Richter, J. Dufouleur, *Nano Lett.* **2021**, *22*, 3550.
[61] Y. Xun, Z. Zhu, X. Chen, J. Qi, *Phys. Rev. B* **2021**, *104*, 085429.
[62] G. Pascal, W. Myung-Hwan, M. Alain, R. Jean, *Inorg. Chem.* **1983**, *23*, 1221.
[63] Y. Zhang, L.-F. Lin, A. Moreo, S. Dong, E. Dagotto, *Physical Review B* **2020**, *101*, 174106.
[64] S. Chae, A. J. Siddiqa, B. J. Kim, S. Oh, K. H. Choi, K. H. Lee, H. Y. Kim, H. K. Yu, J. Y. Choi, *RSC Adv.* **2018**, *8*, 35348.
[65] S. Chae, A. J. Siddiqa, S. Oh, B. J. Kim, K. H. Choi, W. S. Jang, Y. M. Kim, H. K. Yu, J. Y. Choi, *Nanomaterials* **2018**, *8*, 794.
[66] J. Canet-Ferrer, E. Coronado, A. Forment-Aliaga, E. Pinilla-Cienfuegos, *Nanotechnology* **2014**, *25*, 395703.
[67] P. E. Blochl, *Phys Rev. B* **1994**, *50*, 17953.
[68] J. P. Perdew, K. Burke, M. Ernzerhof, *Phys Rev Lett.* **1996**, *77*, 3865.
[69] G. Kresse, J. Hafner, *Phys Rev B Condens Matter* **1993**, *48*, 13115.
[70] G. Kresse, J. Furthmüller, *Phys Rev B Condens Matter* **1996**, *54*, 11169.
[71] S. Grimme, *J. Comput. Chem.* **2006**, *27*, 1787.
[72] A. Togo, F. Oba, I. Tanaka, *Phys Rev B Condens Matter Mater Phys* **2008**, *78*, 134106.
[73] T. J. Boerner, S. Deems, T. R. Furlani, S. L. Knuth, J. Towns, in PEARC 2023 – Computing for the Common Good: Practice and Experience in Advanced Research Computing, Association For Computing Machinery, Inc **2023**, 173.